5

The high mass end of the Tully-Fisher relation

ABSTRACT — We study the location of our massive early-type disk galaxies on the Tully-Fisher relation. Using a combination of our own data and those from Verheijen (2001), we show that in traditional formulations of the TF relation (using the width of the global HI profile or the maximum rotation velocity), early-type disk galaxies with rotation velocities larger than 200 km/s lie systematically to the right of the relation defined by the less massive systems, causing a characteristic 'kink' in the relations.
We also show that the change in slope largely disappears when we use the asymptotic rotation velocity as kinematic parameter and that the remaining deviations from linearity can be removed when we simultaneously use the total baryonic mass (stars + gas) instead of the optical or near-infrared luminosity. Our results strengthen the view that the Tully-Fisher relation fundamentally links the mass of dark matter haloes with the total baryonic mass embedded in them.

5.1 Introduction

The notion of a tight correlation between absolute luminosities of spiral galaxies and their rotational velocities has been with us for almost thirty years now (Tully & Fisher 1977) and has been confirmed to hold over many decades in luminosity (Courteau 1997; McGaugh et al. 2000; Verheijen 2001, hereafter V01) and in different galaxy environments (Giovanelli et al. 1997; Willick 1999). Courteau et al. (2003) showed that the presence of a bar does not influence the location of a galaxy on the 'Tully-Fisher' (TF) relation either. Galaxies of different morphological types do follow different TF relations (Roberts 1978; Rubin et al. 1985; Hinz et al. 2001; Mathieu et al. 2002; Russell 2004), but these offsets disappear almost entirely when using, instead of optical luminosities, near-infrared photometry (Aaronson & Mould 1983; Peletier & Willner 1993), indicating that most of the differences at bluer wavelengths can be attributed to variations in star formation history along the Hubble sequence and the resulting differences in stellar populations.

The Tully-Fisher relation has become one of the most widely used relations in extragalac-

tic astronomy. It has been commonly used as a powerful tool to estimate distances to galaxies (e.g. Tully & Pierce 2000, and references therein). As a statistical correlation between fundamental properties of spiral galaxies, it has also been used to constrain numerical simulations of galaxy formation (Dalcanton et al. 1997; Navarro & Steinmetz 2000; Bullock et al. 2001), probe galaxy evolution on cosmological timescales (Vogt et al. 1997; Ziegler et al. 2002; Milvang-Jensen et al. 2003; Böhm et al. 2004), or study the structure and stellar populations of nearby galaxies (Courteau & Rix 1999; Bell & de Jong 2001).

Our results regarding the shape of the rotation curves in massive early-type disk galaxies, described in section 4.6, raise the question where such galaxies lie on the Tully-Fisher relation as defined by later-type spiral galaxies. Peletier & Willner (1993) noted that the TF relation seems to 'turn over' above rotation velocities of about 225 km/s. Similarly, V01 showed, based on a sample of 31 galaxies in the Ursa-Major cluster with well-defined rotation curves and K-band photometry, that galaxies with declining rotation curves (typically bright systems with high rotation velocities) lie systematically on the high velocity side of the relation defined by galaxies with flat rotation curves, when using the maximum rotation velocity $V_{\rm max}$ or the inclination corrected width of the HI profile. Clearly, the existence of a change in slope of the Tully-Fisher relation has important consequences and, if not corrected for, will lead to systematic biases when deriving cosmological distances or probing galaxy evolution.

However, V01 also showed that the systematic offset at the high mass end disappeared when the rotation velocities $V_{\rm asymp}$ in the outer, flat parts of the rotation curves were used. Bearing in mind that the asymptotic rotation velocities are determined by the dark matter haloes, V01 interpreted his results as a strong indication that the TF relation fundamentally links the total baryonic content of (disk) galaxies with their dark matter haloes, and that as far as this relation is concerned, there is no fundamental difference between low and high mass galaxies. Unfortunately, Verheijen's sample only contained a small number of galaxies with declining rotation curves and the declines were only small. Our sample contains many galaxies with strongly declining rotation curves where the difference between the maximum and asymptotic rotation velocities is much larger than in Verheijen's galaxies. It therefore enables us to investigate the relation between the rotation curve shapes and the change in slope at the bright end of the TF relation much better. In this chapter, we combine our sample of rotation curves from chapter 4 with the data for the galaxies with flat and declining rotation curves from V01 to study the TF relation over 2 decades of luminosity (~5 magnitudes).

The outline of this chapter is as follows. In section 5.2, we describe the B-, R-, I- and K-band photometric data used for the analysis and the corrections which were applied to correct for internal extinction. The kinematic data are described in section 5.3. In section 5.4, we present the Tully-Fisher relations and show that there is indeed a change in slope around 200 km/s. In section 5.5, we discuss the location of the massive, early-type disk galaxies on the Baryonic Tully-Fisher relation. Finally, we summarize our results and draw some conclusions in section 5.6.

5.2 Photometric data for the TF analysis

In chapter 3, we derived absolute magnitudes and errors for our galaxies in B and R; for 5 galaxies, I-band photometry was available as well. In a few cases, however, the magnitudes in chapter 3 were derived from observations on non-photometric nights. Although it was

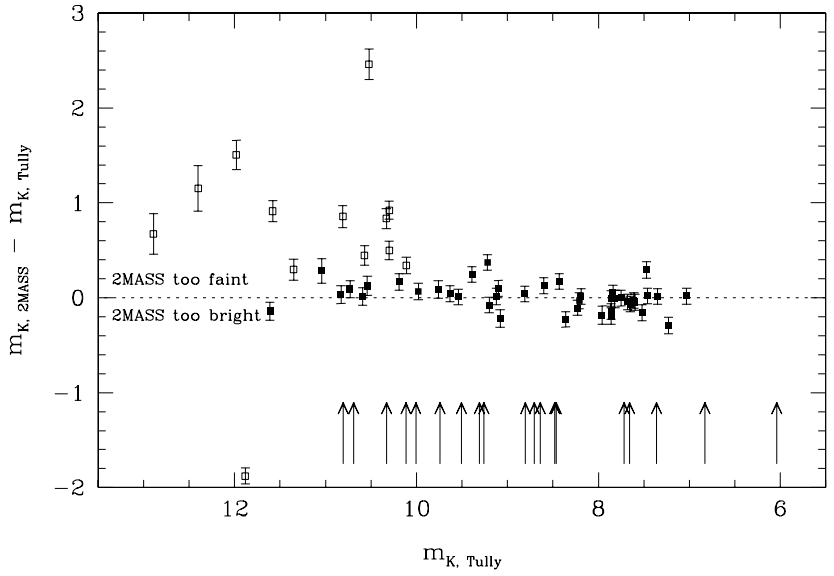

Figure 5.1: *Comparison of 2MASS K-band magnitudes with the data from T96. Data points show the difference between the total apparent magnitudes from 2MASS and those from T96; errorbars show the combined errors. Open symbols indicate low surface brightness galaxies ($\mu_{0,K} > 18$ mag arcsec^{-2}), filled symbols indicate HSB systems. Vertical arrows indicate the 2MASS apparent magnitudes for the galaxies in the present sample.*

attempted to include the resulting photometric calibration uncertainties into the errors, those data lack the reliability required for the present study, and were therefore rejected here.

V01 also had K-band photometry at his disposal. We did not observe our galaxies in the near-infrared, but all galaxies in our sample were observed in K in the framework of the Two Micron All Sky Survey*. To judge the reliability of the 2MASS photometric data, we compared the K-band magnitudes from Tully et al. (1996, hereafter T96) with the total extrapolated magnitudes from 2MASS; the results are shown in figure 5.1. This figure clearly shows that the 2MASS photometric data are reliable for high surface brightness (HSB) galaxies. For the galaxies with measured central surface brightness $\mu_{0,K} < 18.0$ mag arcsec^{-2}, the average difference between 2MASS' and T96's magnitudes is 0.01 mag, with a standard deviation of 0.14 mag. V01 reported, based on an internal comparison of their observations from different nights, an average photometric uncertainty of 0.08 mag in the K-band magnitudes of T96. This implies that the uncertainties in the 2MASS magnitudes must be approximately 0.11 mag, significantly larger than the average errors given by the 2MASS database (0.03 mag for the HSB galaxies in figure 5.1). Photometric errors of 0.03 mag seem somewhat optimistic, in particular since the 2MASS images are significantly less deep than those of T96.

Figure 5.1 also shows that for low surface brightness galaxies, the 2MASS magnitudes are not reliable and sometimes deviate strongly from the values from T96. Inspection of the

*2MASS: http://www.ipac.caltech.edu/2mass/

2MASS images for these galaxies shows that they are of such low surface brightness that they are often barely detected (in fact, most of the LSB galaxies from Tully's sample are not detected at all by 2MASS). Apparently, 2MASS has missed a large fraction of the flux of many LSB galaxies, compared to the deeper data from T96.

The galaxies from the present sample are all early-type disk galaxies of high surface brightness. For these galaxies, it seems safe to adopt the 2MASS magnitudes, but we assume an average photometric uncertainty of 0.11 mag instead of the smaller errors given by 2MASS. The 2MASS apparent magnitudes were converted to absolute magnitudes using the distances from table 2.3 and the corrections for galactic foreground extinction from Schlegel et al. (1998).

The absolute magnitudes in the four bands have not yet been corrected for internal extinction caused by dust in the galaxies themselves. Several correction schemes exist to determine the amount of internal extinction; the most commonly used methods are based on those of Tully & Fouqué (1985) or Giovanelli et al. (1994). Here, we follow V01, who employed the following relation, originally derived by Tully et al. (1998), for the internal extinction parameter:

$$A_\lambda^{i\to 0} = -\gamma_\lambda \log\left(\frac{b}{a}\right), \tag{5.1}$$

with b/a the observed minor-to-major axis ratio of the optical image. γ_λ is wavelength dependent and was found by Tully et al. (1998) to depend also on the absolute luminosity of the galaxy: brighter galaxies contain on average more dust than fainter ones. These authors use the Tully-Fisher relation itself, in an iterative way, to express the absolute luminosity in terms of the HI line width, and give the following description for γ_λ:

$$\gamma_\lambda = \alpha_\lambda + \beta_\lambda(\log W_{20,R}^{c,i} - 2.5), \tag{5.2}$$

where $W_{20,R}^{c,i}$ is the HI line width, corrected for inclination and broadening due to instrumental effects and random gas motions (see below). For the wavelength dependent parameters α_λ and β_λ, we use the values given by Tully et al. (1998).

In table 5.1, we give for each galaxy the raw apparent magnitudes, the galactic foreground and internal extinction parameters, $A_\lambda^{\rm fg}$ and A_λ^i, and the resulting corrected absolute magnitudes used in the remainder of this chapter. The table shows that the internal extinction corrections can be quite substantial, up to one magnitude in the B-band for highly-inclined galaxies such as UGC 8699. Even in the K-band, the corrections are significant, although they do not exceed 0.1 magnitude except in the most inclined systems.

The errors in columns (2) and (6) of table 5.1 are photometric errors only. In addition to these errors, we also account for the distance uncertainties by assuming a typical peculiar velocity of 200 km/s; the resulting error on the absolute magnitude $\delta M_{\rm dist}$ is given in column (11) of table 5.1 and was added quadratically to the photometric errors to obtain the total uncertainties used for the subsequent analysis. V01 does not give individual errors on the magnitudes of his galaxies, but only gives an average photometric uncertainty of 0.05 mag in B, R and I and 0.08 mag in K, and a distance uncertainty of 0.17 mag. We simply adopt these uncertainties for all galaxies from his sample here, but note that individual galaxies may have larger deviations.

We have not included the uncertainties in the internal extinction corrections in our error budget here. Especially for the optical magnitudes of the highly-inclined systems in our samples, the corrections A_λ^i are large and galaxy-to-galaxy variations of γ_λ can cause substantial

deviations from the corrections used here. However, without additional information about the dust content of our galaxies, the corrections listed in table 5.1 are the best possible estimate and the uncertainties are very difficult to quantify. We will ignore these uncertainties for the subsequent analysis here, but note that some of the scatter in our TF relations might be explained by the uncertainties in the internal extinction.

5.3 Kinematic data for the Tully-Fisher analysis

We use three kinematic parameters for our Tully-Fisher analysis. The first is the inclination corrected width of the HI line profile. The profile widths given in chapter 2 were already corrected for instrumental broadening. Here, we apply an additional correction for broadening of the profiles caused by random gas motions in the gas disks. We use the corrections given by Verheijen & Sancisi (2001, based on Tully & Fouqué 1985):

$$\left(W^c_{20,R}\right)^2 = \left(W^c_{20}\right)^2 \; + \; W_t^2 \left[1 - 2e^{-\left(\frac{W^c_{20}}{W_c}\right)^2}\right] \; - \; 2W^c_{20} W_t \left[1 - e^{-\left(\frac{W^c_{20}}{W_c}\right)^2}\right], \qquad (5.3)$$

with W^c_{20} taken from table 2.3. W_c indicates the profile width where the transition from a Gaussian to a boxy shape occurs; we assume here $W_c = 120$ km/s (de Vaucouleurs et al. 1983). In practice, all our galaxies have profile widths larger than W_c, such that equation 5.3 yields a linear subtraction of W_t, which gives the amount by which a profile is broadened due to the random gas motions. Verheijen & Sancisi (2001) present an extensive discussion about the suitable choice for W_t; here we simply copy their preferred value of $W_t = 22$ km/s. The derived profile widths $W^c_{20,R}$ were corrected for inclination using the values given in table 4.3; for warped galaxies we use the inclination in the inner regions where most of the gas is concentrated.

The two other kinematic parameters are the maximum rotation velocity $V_{\rm max}$ and the asymptotic rotation velocity $V_{\rm asymp}$, which are both derived directly from the rotation curves (see section 4.3.3). The rotation curve of UGC 11914 only extends out to about 3.3 R-band disk scale lengths and does not show the characteristic decline that we see in other galaxies of similar type and luminosity (see section 4.8 and appendix 4-I). Since in many other cases, the decline in the rotation velocities sets in outside the optical disk only, it is well possible that the rotation curve in UGC 11914 would also decline at larger radii if we were able to measure it. The asymptotic rotation velocity $V_{\rm asymp}$ for UGC 11914 seems therefore ill-defined and we excluded this galaxy from the sample for the asymptotic velocity relations.

The errors on the profile widths are dominated by the uncertainties in inclination, which were derived in section 4.3.1. The errors on the two other kinematic parameters were estimated by eye, based on the errors in the rotation curves (see section 4.3.4). They include contributions from measurement errors, kinematic asymmetries and inclination uncertainties; for the more face-on galaxies, the latter are usually dominant.

All three kinematic parameters and corresponding errors for each galaxy are given in table 5.1. The kinematic parameters and corresponding errors from V01 were copied here without further modifications.

5.4 Tully-Fisher relations

In figure 5.2, we show the Tully-Fisher relations for the samples from this study (open circles) and from V01 (solid dots), for the four available photometric bands and three kinematic

Table 5.1: *Photometric and kinematic properties used for the Tully-Fisher analysis: (1) UGC number; (2), (6) total apparent magnitudes and errors, taken from chapter 3 (B, R and I) and the 2MASS galaxy catalogue (K); (3), (7) correction for galactic foreground extinction, taken from Schlegel et al. (1998); (4), (8) correction for internal extinction, calculated using equation 5.1; (5), (9) resulting absolute magnitudes; (10) assumed distance, taken from chapter 2; (11) magnitude error due to distance uncertainties; (12) maximum and asymptotic rotation velocities, taken from chapter 4; (13) width of global HI profile, taken from chapter 2, corrected for instrumental broadening, random gas motions and inclination.*

UGC	m_B / m_R	A_B^{fg} / A_R^{fg}	A_B^i / A_R^i	M_B^c / M_R^c	m_I / m_K	A_I^{fg} / A_K^{fg}	A_I^i / A_K^i	M_I^c / M_K^c	D	δM_{dist}	V_{max} / V_{asymp}	$W_{20,R}^{c,i}$
		mag				mag			Mpc	mag	km/s	
(1)	(2)	(3)	(4)	(5)	(6)	(7)	(8)	(9)	(10)	(11)	(12)	(13)
624	13.48 ± 0.03	0.24	0.74	-21.57	11.23 ± 0.07	0.11	0.44	-23.38	65.1	0.09	300 ± 16	599 ± 38
	11.96 ± 0.05	0.15	0.53	-22.78	9.26 ± 0.11	0.02	0.11	-24.94			270 ± 30	
2487	13.06 ± 0.10	0.79	0.25	-22.13	–	–	–	–	67.4	0.09	390 ± 21	755 ± 36
	11.39 ± 0.03	0.49	0.18	-23.42	8.64 ± 0.11	0.07	0.04	-25.61			330 ± 24	
2916	14.18 ± 0.03	1.21	0.14	-21.19	–	–	–	–	63.5	0.09	220 ± 17	501 ± 39
	12.75 ± 0.06	0.75	0.10	-22.11	10.01 ± 0.11	0.10	0.02	-24.13			180 ± 17	
2953	11.49 ± 0.16	1.82	0.41	-21.63	8.34 ± 0.16	0.82	0.24	-23.61	15.1	0.38	315 ± 9	603 ± 18
	–	–	–	–	6.04 ± 0.11	0.15	0.06	-25.07			260 ± 16	
3205	14.88 ± 0.18	2.33	0.79	-21.68	12.01 ± 0.21	1.05	0.47	-22.95	48.7	0.12	240 ± 7	451 ± 7
	13.00 ± 0.12	1.45	0.57	-22.45	9.50 ± 0.11	0.20	0.11	-24.24			210 ± 5	
3546	12.47 ± 0.22	0.31	0.38	-20.40	–	–	–	–	27.3	0.21	260 ± 65	421 ± 13
	11.02 ± 0.03	0.19	0.28	-21.63	8.48 ± 0.11	0.03	0.05	-23.78			190 ± 12	
3580	13.33 ± 0.02	0.23	0.36	-18.67	–	–	–	–	19.2	0.30	127 ± 5	246 ± 7
	12.14 ± 0.05	0.14	0.27	-19.69	10.12 ± 0.11	0.02	0.05	-21.37			125 ± 5	
3993	14.04 ± 0.20	0.28	0.08	-20.27	–	–	–	–	61.9	0.09	300 ± 45	550 ± 79
	12.78 ± 0.16	0.17	0.06	-21.41	10.33 ± 0.11	0.02	0.01	-23.66			250 ± 40	
4458	12.81 ± 0.18	0.15	0.13	-21.51	–	–	–	–	64.2	0.09	490 ± 75	620 ± 93
	11.52 ± 0.10	0.09	0.09	-22.70	9.31 ± 0.11	0.01	0.02	-24.76			240 ± 43	

Table 5.1: *Photometric and kinematic properties used for the Tully-Fisher analysis:* continued

UGC	m_B m_R	$A_B^{\rm fg}$ $A_R^{\rm fg}$	A_B^i A_R^i	M_B^c M_R^c	m_I m_K	$A_I^{\rm fg}$ $A_K^{\rm fg}$	A_I^i A_K^i	M_I^c M_K^c	D	$\delta M_{\rm dist}$	$V_{\rm max}$ $V_{\rm asymp}$	$W_{20,R}^{c,i}$
		mag				mag			Mpc	mag	km/s	
(1)	(2)	(3)	(4)	(5)	(6)	(7)	(8)	(9)	(10)	(11)	(12)	(13)
4605	– –	– –	– –	– –	– 8.46 ± 0.11	– 0.02	– 0.14	– -23.30	20.9	0.28	225 ± 5 185 ± 4	412 ± 2
5253	– 9.79 ± 0.24	– 0.07	– 0.13	– -22.03	– 7.36 ± 0.11	– 0.01	– 0.03	– -24.30	21.1	0.27	255 ± 20 210 ± 21	495 ± 34
6786	– 11.02 ± 0.06	– 0.08	– 0.58	– -21.71	– 8.70 ± 0.11	– 0.01	– 0.11	– -23.48	25.9	0.22	230 ± 5 215 ± 10	456 ± 6
6787	11.47 ± 0.11 10.16 ± 0.26	0.09 0.06	0.60 0.43	-20.60 -21.71	– 7.66 ± 0.11	– 0.01	– 0.08	– -23.82	18.9	0.31	270 ± 10 250 ± 7	495 ± 7
8699	13.39 ± 0.11 12.11 ± 0.24	0.04 0.03	0.94 0.68	-20.42 -21.42	– 9.74 ± 0.11	– 0.00	– 0.13	– -23.22	36.7	0.16	205 ± 6 180 ± 9	382 ± 10
9133	12.52 ± 0.09 11.09 ± 0.09	0.07 0.04	0.44 0.32	-21.66 -22.94	– 8.80 ± 0.11	– 0.01	– 0.06	– -24.94	54.3	0.11	300 ± 15 225 ± 12	537 ± 18
11670	– 10.55 ± 0.11	– 0.58	– 0.46	– -21.01	9.81 ± 0.14 7.72 ± 0.11	0.42 0.08	0.37 0.09	-21.50 -22.97	12.7	0.46	190 ± 5 160 ± 6	341 ± 6
11852	14.38 ± 0.10 13.17 ± 0.08	0.30 0.19	0.38 0.28	-20.82 -21.81	12.51 ± 0.09 10.69 ± 0.11	0.14 0.03	0.23 0.05	-22.37 -23.90	80.0	0.07	220 ± 16 165 ± 11	401 ± 29
11914	10.98 ± 0.24 9.75 ± 0.22	0.38 0.24	0.11 0.08	-20.38 -21.43	– 6.83 ± 0.11	– 0.03	– 0.01	– -24.08	14.9	0.39	305 ± 43 –	583 ± 85
12043	13.68 ± 0.12 12.85 ± 0.26	0.28 0.17	0.37 0.28	-17.90 -18.54	– 10.81 ± 0.11	– 0.02	– 0.05	– -20.21	15.4	0.38	93 ± 6 90 ± 4	185 ± 3

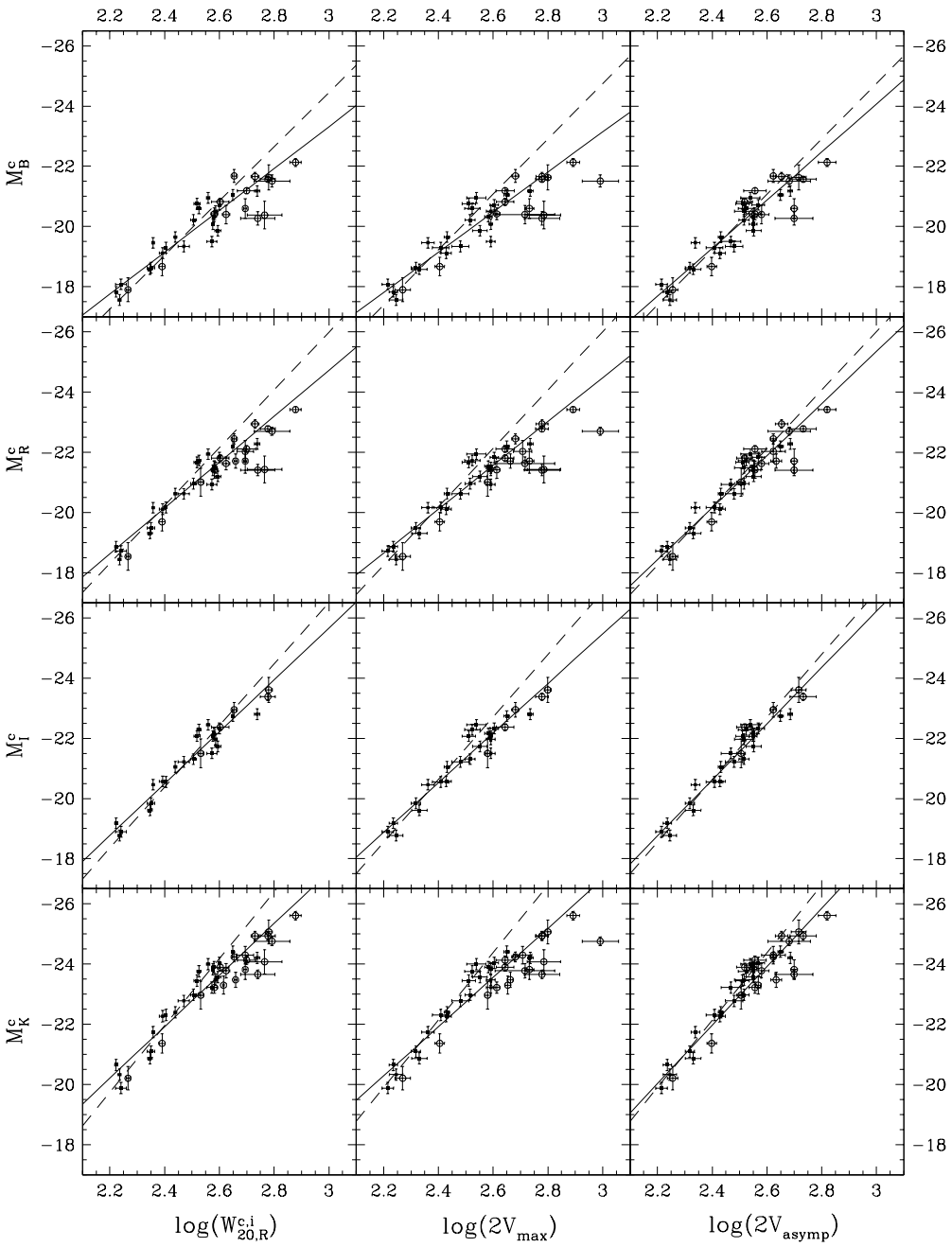

Figure 5.2: *Tully-Fisher relations in B-, R-, I- and K-band (*top to bottom*), using the corrected widths of the global* H I *profiles (*left*) and the maximum (*middle*) and asymptotic rotation velocities (*right*). Open circles indicate the galaxies from the present sample, dots show galaxies with flat or declining rotation curves from V01. The full lines show the fits to the combined sample, the dashed lines shows the fits from V01 to galaxies with flat rotation curves.*

Table 5.2: *Results from the least-χ^2 fits to the Tully-Fisher relations shown in figure 5.2:*

kinematic parameter	band	# of points	zero point	slope	scatter	$\chi^2_{\rm red}$	Q
			mag		mag		
$W^{c,i}_{20,R}$	B	37	-2.44 ± 0.56	-6.96 ± 0.23	0.41	3.62	$1.8 \cdot 10^{-13}$
	R	39	-1.81 ± 0.56	-7.64 ± 0.22	0.35	2.60	$6.0 \cdot 10^{-8}$
	I	27	0.19 ± 0.69	-8.62 ± 0.29	0.34	2.56	$5.0 \cdot 10^{-6}$
	K	41	-1.38 ± 0.60	-8.56 ± 0.24	0.41	2.98	$1.7 \cdot 10^{-10}$
$V_{\rm max}$	B	37	-3.13 ± 0.61	-6.67 ± 0.23	0.44	3.29	$1.6 \cdot 10^{-11}$
	R	39	-2.64 ± 0.62	-7.28 ± 0.24	0.38	2.26	$4.7 \cdot 10^{-6}$
	I	27	-0.75 ± 0.77	-8.24 ± 0.30	0.32	1.62	$1.2 \cdot 10^{-2}$
	K	41	-2.34 ± 0.67	-8.16 ± 0.25	0.44	2.60	$3.2 \cdot 10^{-8}$
$V_{\rm asymp}$	B	36	-0.13 ± 0.78	-7.98 ± 0.30	0.42	2.42	$1.4 \cdot 10^{-6}$
	R	38	0.60 ± 0.77	-8.65 ± 0.31	0.36	1.65	$3.8 \cdot 10^{-3}$
	I	27	1.77 ± 0.93	-9.33 ± 0.36	0.31	1.24	$1.2 \cdot 10^{-1}$
	K	40	1.33 ± 0.81	-9.71 ± 0.33	0.40	1.78	$8.7 \cdot 10^{-4}$
$V_{\rm asymp}$ (UGC 3993 and 6787 excluded)	B	34	0.38 ± 0.80	-8.17 ± 0.31	0.39	2.13	$5.7 \cdot 10^{-5}$
	R	36	0.85 ± 0.82	-8.77 ± 0.32	0.33	1.41	$3.2 \cdot 10^{-2}$
	I	27	1.77 ± 0.93	-9.33 ± 0.36	0.31	1.24	$1.2 \cdot 10^{-1}$
	K	38	1.73 ± 0.87	-9.90 ± 0.34	0.37	1.50	$1.4 \cdot 10^{-2}$

parameters. In the I-band, our study only adds 5 data points to Verheijen's sample, but two of those (UGC 624 and 2953) are about 0.7 magnitudes more luminous than his brightest galaxies, so our data still form a relevant addition to his sample. In the other bands, our data greatly increase the number of luminous galaxies, with our most luminous system, UGC 2487, being 1.2 magnitudes brighter in K than the most luminous object in Verheijen's sample.

The solid lines in the figure indicate the results from least-χ^2 fits to the combined sample. The results of these fits are summarized in table 5.2. The scatter around each of the fits given in this table is a weighted rms scatter, with the weight for each data point given by $w_i = (\sigma^2_{Mi} + s^2\sigma^2_{\log Vi})^{-1}$. Here, σ_{Mi} are the magnitude errors, $\sigma_{\log Vi}$ are the errors in the parameters on the x-axes and s are the fitted slopes of the relations. Thus, we take the errors in both directions into account. For comparison, we also show with dashed lines the fits to the 'F'-sample from V01, i.e. the fits made to galaxies with flat rotation curves only.

A number of interesting results can be recognised from figure 5.2 and table 5.2. First of all, our data strongly suggest a 'kink' in the Tully-Fisher relation: the TF relation seems to become shallower above a rotation velocity of about 200 km/s (equivalent to $M^c_R < -21.5$). This is consistent with the claim first made by Peletier & Willner (1993), but the effect is much more clearly visible here than in their data. The kink is most apparent when using the width of the global profile ($W^{c,i}_{20,R}$) or the maximum rotation velocity $V_{\rm max}$ as kinematic parameter. In the left and middle panels in the figure, almost all galaxies from our sample lie to the right of the relation defined by the later-type galaxies with flat rotation curves from V01. As a result, the fits to the combined samples have a shallower slope than those to the galaxies with flat rotation curves from Verheijen.

However, the turnover is greatly reduced when using the asymptotic rotation velocity $V_{\rm asymp}$ as kinematic parameter. Many of the galaxies in our sample with $V_{\rm max} > 200$ km/s have strongly declining rotation curves (see section 4.6). Galaxies such as UGC 4458, 4605, 3546, which lie far to the right of the main relation in the left and middle panels, shift to the left when the (lower) asymptotic velocity is used, thereby straightening the TF relation. This effect is also reflected in the values for the rms scatter and χ^2 of the data around the fits and the 'goodness-of-fit' parameters Q. Table 5.2 shows that the TF relations using $V_{\rm asymp}$ are much better represented by straight lines than the relations with the other two parameters. However, the kink does not disappear completely. Even in the right hand panels of figure 5.2, most galaxies at the bright end lie to the right of the relation defined by the less luminous galaxies with flat rotation curves from V01, indicating that the slope of the TF relation also changes when the asymptotic rotation velocities $V_{\rm asymp}$ are used.

We confirm the results from previous studies (e.g. Pierce & Tully 1992; Tully & Pierce 2000; Verheijen 2001) concerning the colour-dependencies in the Tully-Fisher relation. The TF relation steepens when going from blue to red bands. The fact that our I-band TF relations using $W^{c,i}_{20,R}$ or $V_{\rm max}$ are slightly steeper than the corresponding K-band relations, can be explained by the small number of galaxies from our own sample with I-band photometry. Inclusion of more galaxies with declining rotation curves at the top end of the I-band relations would probably flatten their slopes to values between the R- and K-band slopes. Note that in the relations using $V_{\rm asymp}$, there is a steady increase in the slopes from B to K.

The scatter in our relations using the asymptotic rotation velocities is systematically larger than the corresponding values found by V01. This difference can partly be attributed to the fact that Verheijen's galaxies all lie in the Ursa-Major cluster, such that the distance uncertainties are small (at least in a relative sense). Our galaxies lie predominantly in the field, where peculiar motions with respect to the Hubble flow lead to errors in the derived distances and absolute luminosities (see table 5.1), and thus to additional scatter in the TF relations. More importantly however, the scatter in our relations is artificially increased by the deviations from a straight line. Even in the relations using the asymptotic rotation velocity $V_{\rm asymp}$, the kink around 200 km/s causes systematic deviations from the fitted straight lines. Since V01 had only 2 galaxies with $V_{\rm asymp} > 200$km/s, the change in slope at the high mass end had virtually no influence on the scatter around the fits for his data. Note also that the scatter and χ^2 are smallest for our I-band data (and that the corresponding 'goodness-of-fit' parameter Q is highest), where our study only adds 3 data points to Verheijen's data above 200 km/s.

Finally, the scatter in the relations with $V_{\rm asymp}$ is heavily influenced by two galaxies with unusually large deviations from the main relation: UGC 3993 and UGC 6787. In figure 5.3, we show the deviations of the galaxies from our sample with respect to the R-band vs. $V_{\rm asymp}$ fit described in table 5.2. The errorbars in the figure take the uncertainties of the points in both directions into account, and were calculated as $\Delta_{\rm eff} = \sqrt{[\Delta \log(2V)]^2 + [\Delta M/ - 8.65]^2}$, with -8.65 the slope of the fit. UGC 3993 is a nearly face-on galaxy ($i \approx 20°$), with correspondingly large uncertainties in the derived rotational velocities (also reflected in the large errorbars in figures 5.2 and 5.3). The deviation of this galaxy may partly be caused by a slight under-estimation of the true inclination angle. It seems unlikely, however, that the inclination uncertainty is responsible for the full deviation of UGC 3993; to bring this galaxy to the middle of the relation would require an inclination angle of 30°, a value which seems to fall outside the range supported by our data (see the figure in appendix 4-I). The most likely

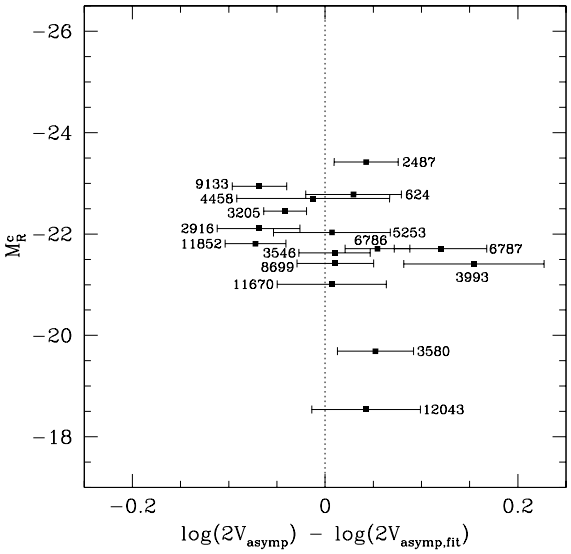

Figure 5.3: *Deviations of the galaxies from the present sample with respect to the R-band vs. V_{asymp} TF relation from table 5.2. Galaxies are numbered according to their UGC numbers. Errorbars are the effective errors, calculated by combining the magnitude and velocity uncertainties (see text).*

explanation for the offset of UGC 6787 from the main relation lies in the distance determination. UGC 6787 lies close to the center of the Ursa Major cluster, but has a redshift that is about 200 km/s higher than the high velocity envelope of the cluster (Tully et al. 1996). It may thus lie behind the main cluster, which might in turn imply that it is being drawn into the cluster and that the recession velocity is lower than expected in the case of pure Hubble flow. In that case, our adopted distance of 18.9 Mpc and the derived luminosities are too small, explaining the offset in the TF relations.

For completeness, we also list in table 5.2 the results of fits to the TF relations with the asymptotic rotation velocities when UGC 3993 and 6787 are excluded from the sample. It is clear that the exclusion of the two points from the fits does not lead to significantly different slopes or zeropoints. As expected, the scatter is reduced, but since the kink in the relations has not been removed by the exclusion of the two discrepant points, the values are still larger than the corresponding ones from V01 and the χ^2 and Q-parameter indicate that the deviations from a straight relation are still real.

5.5 The Baryonic Tully-Fisher relation

What could be the origin of the change of slope in the Tully-Fisher relation? Does it truly indicate a break in the relation between baryons and dark matter, or could it be explained by other effects? In this context, it is interesting to consider the so-called 'Baryonic Tully-Fisher relation', first discussed by McGaugh et al. (2000, see also McGaugh 2005). They showed that there exists another break in the Tully-Fisher relation at the low luminosity end (around V_{rot} = 90 km/s), below which galaxies are also under-luminous. They were, however, able to restore a linear TF relation when, instead of using the stellar luminosity, they adopted the total observed baryonic mass (stars and gas). Since dwarf galaxies contain on average more gas than higher-luminosity spirals, the former shifted upwards more than the latter, and the break in the Tully-Fisher relation disappeared.

In chapter 2, we have shown that the early-type disk galaxies in the present sample have

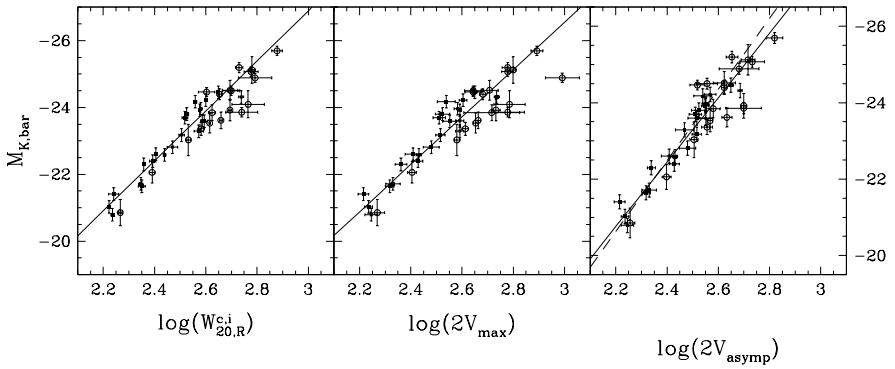

Figure 5.4: *Baryonic Tully-Fisher relation in the K-band. The total gas mass in each galaxy was converted to K-band luminosity, assuming a mass-to-light ratio of the stars of 0.8 (see text). Open circles indicate the galaxies from the present sample, dots show galaxies from V01. The full lines show the fits to the combined sample, the dashed line in the right hand panel shows the fit from V01.*

a wide range in relative gas masses and that some of our systems are very gas-poor. In such galaxies, the baryonic budget is dominated by the stars and adding the gas contribution will not lead to a significant increase in magnitude. In this section, we investigate whether the observed break at the high mass end in our Tully-Fisher relations can be explained as a result of the relatively low gas-content of early-type disk galaxies.

We have converted the total gas masses for the galaxies from the present sample (table 2.3) and those from V01 to K-band luminosities, assuming an average mass-to-light ratio of the stellar populations of 0.8: $L_{K,\mathrm{gas}} = 1.43 M_{\mathrm{HI}}/(M_*/L_K)$, where the factor 1.43 was used to account for the presence of helium. The choice of $M_*/L_K = 0.8$ was made following McGaugh et al. (2000), and is consistent with the average values found from maximum-disk fits from Verheijen (1997) and Palunas & Williams (2000). In reality, the values of M_*/L_K are expected to vary from galaxy to galaxy, but the variations will be modest in the K-band and the adopted average value will suffice for the statistical approach taken here.

The equivalent K-band luminosities of the gas were added to the total stellar luminosities and absolute baryonic magnitudes were calculated according to $M_{K,\mathrm{bar.}} = -2.5 \log[(L_{K,\mathrm{stars}} + L_{K,\mathrm{gas}})/L_\odot] + M_{K,\odot}$. The resulting baryonic TF relations are shown in figure 5.4 for the same three kinematic parameters as used before; the resulting least-χ^2 fits are summarized in table 5.3.

Due to the relatively high gas content of low luminosity galaxies and the gas deficiency in high luminosity systems, the former shift up more than galaxies at intermediate luminosities, and the latter less, such that the baryonic Tully-Fisher relations have a shallower slope than the standard stellar TF relations. More importantly, the 'kink' in the TF relations from figure 5.2 is reduced. The relations with $W^{c,i}_{20,R}$ and V_{max} are better represented by a straight line than the original relations in figure 5.2; the scatter and χ^2 are reduced with respect to the original values and the Q-parameters are increased. In the case of the relation with the asymptotic rotation velocity V_{asymp}, the small 'kink' which was still present in the bottom right hand panel in figure 5.2 seems to have disappeared almost completely now, but at the

Table 5.3: *Results from the least-χ^2 fits to the K-band Baryonic Tully-Fisher relations shown in figure 5.4:*

kinematic parameter	zero point	slope	scatter	$\chi^2_{\rm red}$	Q
	mag		mag		
$W^{c,i}_{20,R}$	-4.45 ± 0.59	-7.48 ± 0.23	0.34	2.23	$4.4 \cdot 10^{-6}$
$V_{\rm max}$	-5.28 ± 0.62	-7.09 ± 0.24	0.39	2.29	$2.0 \cdot 10^{-6}$
$V_{\rm asymp}$	-2.19 ± 0.78	-8.44 ± 0.30	0.40	1.99	$8.9 \cdot 10^{-5}$

same time, the scatter around the mean relation appears to have increased, and the quality of the fit, as measured with the χ^2 and Q-parameter, is actually reduced.

The concept of the Baryonic Tully-Fisher relation may be useful to increase the linearity in the traditional relations with the width of the HI profile or the maximum rotational velocity. Where McGaugh et al. (2000) found that the inclusion of the gas mass straightened the TF relation at the low mass end, our results show that it also reduces the kink around 200 km/s. However, this effect is smaller than the one discussed in the previous section, and the Baryonic Tully Fisher relations using $W^{c,i}_{20,R}$ or $V_{\rm max}$ are still worse than our stellar K-band luminosity vs. $V_{\rm asymp}$ relation shown in figure 5.2 and table 5.2.

The inclusion of the gas also removes the small kink that was still present in the latter relation, and the baryonic K-band vs. $V_{\rm asymp}$ TF relation appears to be fully consistent with a linear relation over the full extent of our data. However, it also introduces additional scatter in the relation and the formal quality of the fit is worse than the original without the gas mass included. The scatter might be reduced if more accurate K-band mass-to-light ratios become available for individual galaxies instead of the constant value of $M_*/L_K = 0.8$ we assumed here, but since these are currently not available, this hypothesis cannot be checked yet.

5.6 Concluding remarks

In the previous sections, we have shown that traditional formulations of the Tully-Fisher relation, using stellar luminosities and the widths of the HI profiles or the maximum rotational velocities, show a characteristic 'break' in the relation around a rotation velocity of about 200 km/s, above which most galaxies rotate faster than expected (or equivalent, are less luminous). This change in slope has important consequences for the use of the Tully-Fisher relation as a tool for estimating distances to galaxies or for probing galaxy evolution. For example, several authors have recently studied the evolution of the Tully-Fisher relation since a redshift of $z \approx 1$. Vogt et al. (1996, 1997) reported that galaxies at redshift $z \sim 1$ were on average 0.6 mag brighter (B-band) than galaxies in the local universe. Ziegler et al. (2002) and Böhm et al. (2004) claimed that the evolution in the Tully-Fisher relation is luminosity dependent, with high mass galaxies ($V_{\rm max} > 150$ km/s) showing little or no evolution, but low mass galaxies being up to 2 magnitudes brighter at high redshift. Our results indicate that high mass galaxies are *under*-luminous in the local universe, compared to a simple extrapolation of the linear relation for lower-luminosity galaxies. Inspection of the B-band luminosity vs. maximum rotational velocity relation (top middle panel) in figure 5.2 shows that this effect can easily be as large as 1 magnitude. Thus, the evolution of the Tully-Fisher relation for high mass galaxies may be much larger than derived by the authors mentioned above.

We have also shown that the 'kink' in the TF relation can be reduced in two different ways, namely *1*) by using the asymptotic rotation velocity from the rotation curve as kinematic parameter and *2*) by adopting the total baryonic mass (stars + gas) as luminosity parameter. The first correction appears to be the most important one for high mass galaxies and the TF relations using the asymptotic rotation velocities show only a small deviation from linearity. However, the inclusion of the gas mass also improves the linearity and only when both refinements are used in conjunction does the 'kink' disappear completely and is a linear relation recovered. Our results seem to be a strong confirmation of the idea that the Tully-Fisher relation is fundamentally a relation between the mass of the dark matter haloes (which define $V_{\rm asymp}$) and the total baryonic mass in galaxies (cf. McGaugh et al. 2000; Verheijen 2001).

Acknowledgements

I would like to thank Mark Verheijen for his help and stimulating discussions during the work which led to the results presented in this chapter.

For the work in this chapter, we made use of data from the Two Micron All Sky Survey, which is a joint project of the University of Massachusetts and the Infrared Processing and Analysis Center/California Institute of Technology, funded by the National Aeronautics and Space Administration and the National Science Foundation.